Korean J. Chem. Eng., 37(9), 1453-1465 (2020)
DOI: 10.1007/s11814-020-0556-8

pISSN: 0256-1115
eISSN: 1975-7220

Fluid flow effects on diffusion layer and current density for electrochemical systems

Behzad Ebadi[*,], Morteza Behbahani-Nejad[*,**,†], Maziar Changizian[*,**], and Ioan Pop[***]**

*Department of Mechanical Engineering, Faculty of Engineering,
Shahid Chamran University of Ahvaz, 61357-83151, Ahvaz, Iran
**Gas Networks Research Center, Shahid Chamran University of Ahvaz, 61357-83151, Ahvaz, Iran
***Department of Mathematics, Faculty of Mathematics and Computer Science,
Babeş-Bolyai University, 400084 Cluj-Napoca, Romania
(*Received 14 November 2019 • Revised 12 March 2020 • Accepted 12 April 2020*)

Abstract−The effects of flow field upon the distribution of ionic concentration, electric potential, concentration boundary layer thickness, and electric current density were investigated. A modified numerical scheme is proposed to simulate the corresponding electrochemical system which is governed by nonlinear partial differential equations. Seven types of geometries and various flow fields with Reynolds numbers up to 2100 are considered. The obtained results indicate the current numerical method can successfully simulate the increase of current density on the cathode as the applied potential cell increases, and that rise will continue until the limiting current density is reached. To predict the effect of fluid flow, the proposed scheme is applied for various Peclet numbers. The increase of current density for Peclet numbers between 1 and 10^4 is quite evident. But for large Peclet numbers between 10^4 and 10^7, the current density increases gradually. The results also show that as the anode size is doubled, the maximum current density occurs at the leading and trailing edges. However, if the cathode size is doubled, the maximum current density occurs at the center regions of it. Knowing the regions where current density is extremum helps electochemical system designers to control the parameters of the corresponding process.

Keywords: Non-linear Coupled Manner, Electrochemical Systems, Diffusion Layer, Butler-Volmer, Fluid Flow

INTRODUCTION

Electrochemical processes are widely applied in various branches of industry, such as batteries, fuel cells, electroplating, cathodic protection, and manufacturing of processor interconnectors. Among these, electroplating is widely used to cover conductive materials by electrical current. The thickness of the electrodeposited layer is a critical factor in the electroplating process [1]. The distribution of deposited thickness across the cathode surface is directly dependent on the distribution of current density [2,3]. In this regard, the current density distribution should be justified in order to reach the desired deposited thickness [4,5]. The leading factors affecting the current density distribution include cell geometry, mass transfer of reacting species, kinetics of the electrochemical reactions at electrodes, and the conductivity of electrolyte [2].

One of the promising means for fundamental understanding of the behavior of electrochemical systems is numerical simulation. The numerical modeling of electrochemical systems not only reduces designing costs but also gives a better insight into the distribution of electrical current on the electrodes. It should be noted that the ionic transport phenomenon plays a decisive role in the electrochemical reactions. Regarding the continuum theory for macro-scale electrochemical models, three ionic transfer mechanisms are highlighted for dilute electrolytes including convection, diffusion and migration [6,7]. In some electrochemical applications, the convection term can be overlooked due to the static nature of electrolyte. However, in the majority of applications, the convection term should be underscored due to the presence of appreciable fluid flow. For instance, the cathodic protection systems of ships moving through the sea water are influenced by forced convection [8]. As an additional example, batteries could be affected through the free convection being formed with concentration gradient on the electrodes realm [9].

The numerical solving of electrochemical equations, in the general form without any simplification, is very cumbersome due to nonlinearity of both the governing equations and the Butler-Volmer boundary condition on electrodes. Moreover, electrochemical applications are typically faced with high Peclet numbers, applying serious convergence difficulties in the electrochemistry modelling [10]. To reduce the complexity, many studies have ignored the convection term or/and diffusion term in modelling different types of electrochemical systems. Ignoring the above terms does not alter the physics of those problems when there is thin diffusion layer or calm electrolyte.

For example, Lorenzi et al. [11] modeled cathodic protection with disregarding effect of convection and diffusion terms. In this case, the nonlinear governing equation reduced to the Laplace's equation for electric potential. Under a thin diffusion layer condition, Lee and Selman [12] simulated an electrochemical zinc-bromine flow reactor with a separator to determine the current distributions at a parallel-plate reactor. Their study demonstrated that an appropriate current tab location (i.e., at the trailing end of the electrode)

†To whom correspondence should be addressed.
E-mail: bnmorteza@scu.ac.ir

could contribute to smoother current distribution. White et al. [13] modelled a closed parallel-plate electrochemical reactor based on the dilute electrolyte theory in which the axial diffusion and migration terms are neglected. The latter assumptions result in formulations which are not suitable for a high inlet velocity.

Using finite volume method, Buoni and Petzold [14] modelled a three-dimensional copper electro-deposition with moving boundaries. In their study, the convection term was not considered. Applying finite element method, Henley and Fisher [15] calculated electric current density distribution for a three-dimensional micro-electrochemical reactor by decoupling the migration-related term from general governing equation. In more detail, they considered Laplace's equation for the migration term and a convection-diffusion equation for the concentration distribution, which are separately solved.

It is of utmost importance that, in the presence of fluid flow, the diffusion layer in electrochemical domain is highly dependent on the flow characteristics. Accordingly, the convection, diffusion, and migration effects should be simultaneously implemented in order to capture the detailed properties of electrochemical domains. However, a handful number of studies have dealt with non-simplified multi-ion transport models. For instance, Bortels et al. [16] involved all the transport effects for simulating a steady state two-dimensional parallel plate electrochemical reactor under fully-developed laminar flow pattern. In this study, the authors applied multi-dimensional upwind method for modeling the electrochemical domain. Georgiadou [17] developed a finite-difference method to simulate ionic transport in a parallel-plate reactor when the convection term is dominant.

In another effort, Nelissen et al. [18] as well as Volgin and Davydov [19] performed multi-ion calculations using finite difference method. These studies mostly concentrated on the theoretical aspect and provided valuable findings about the stability and solving speed of multi-ion equations. Bauer et al. [20] modelled ionic transfer equations with nonlinear boundary conditions. They revealed that the standard Galerkin finite element method led to severe fluctuations in the results where the convection term was dominant. Their study proposed a stabilized finite element method to attain relatively acceptable results without numerical oscillations.

There are two successful strategies, i.e., segregated approach and coupled approach, for numerically computing the discretized equations system. Due to less memory usage and reduced computation time, most commercial electrochemical software employs the segregated approach to solve nonlinear equations. However, the coupled approach has attracted more attention compared to the segregated counterpart, since the former has superior convergence over the latter. Moreover, access to present-day super computers leads to a remarkable increase in the popularity of the coupled solution method. Mazumder [21] comprehensively discussed that the coupled approach achieved an accurate convergence in the majority of the cases that the segregated method was unable to converge.

For this reason, the present study employed the coupled approach for solving the fully coupled nonlinear partial differential equations along with the nonlinear kinetic of electrode in order to investigate the effects of fluid flow effects on a parallel-plate electrochemical reactor. Moreover, this study evaluated the behavior of diffusion layer, electric potential and current distribution for several flow velocities. The thickness of diffusion layer was obtained for different conditions. This can specify the part of electrochemical domain where the Laplace equation for electric potential is valid. In addition, the current density variation on the cathode, as a key parameter for electrochemical systems, is presented at various applied potential cells. Overall, the modified numerical scheme applied here can provide a unifying tool for robust numerical analysis of electrochemical systems interacting with fluid flow.

PROBLEM STATEMENT AND FORMULATION

1. Governing Equations

The basic assumptions in this study involve steady state, dilute electrolyte and constant physical properties. The total flux of each ion (m) including convection, diffusion and migration is presented below:

$$\mathbf{N}_m^{conv+diff+mig} = \mathbf{V}c_m - D_m \nabla c_m - z_m \mu_m F(c_m \nabla \Phi) \tag{1}$$

In the electrochemical literature, Eq. (1) is also referred to as the Nernst-Planck equation. In dilute-solution theory, the absolute mobility μ_m is assumed to be related to the diffusion coefficient D_m according to the Nernst-Einstein relation:

$$\mu_m = \frac{D_m}{RT} \tag{2}$$

Inside the electrolyte, electrical conductivity is extremely high, so it can be assumed that there is no uncompensated charge. Therefore, the electro-neutrality law is expressed as follows:

$$\sum_{m=1}^{p} z_m c_m = 0 \tag{3}$$

The electro-neutrality law is valid throughout the domain, except in areas near the electrodes where the electric double layer exists. The total electric current density can be easily obtained from the summation of each ion flux in combination with electro-neutrality criteria as below:

$$\mathbf{i} = F \sum_{m=1}^{p} z_m \mathbf{N}_m^{diff+mig} \tag{4}$$

Due to the existence of the electro-neutrality condition, the convection term is eliminated from the flux in Eq. (4). The steady state of charge conservation law can be written in this way:

$$-\nabla \cdot \mathbf{N}_m^{conv+diff+mig} + R_m = 0 \tag{5}$$

where R_m is the production rate of each ion that occurs in a homogeneous reaction within the bulk of electrolyte (which can be positive, negative or zero). Inasmuch as the reactions are only restricted to the electrode realm, R_m is zero.

In this study, the dimensionless forms of the governing equations and boundary conditions have been used in order to eliminate numerical difficulties such as convergence instability:

$$\mathbf{N}_m^{* \, conv+diff+mig} = Pe \mathbf{V}^* c_m^* - D_m^* \nabla^* c_m^* - z_m D_m^* c_m^* \nabla^* \Phi^* \tag{6}$$

$$-\nabla^* \cdot \mathbf{N}_m^{* \, conv+diff+mig} = 0$$

$$= [Pe \nabla^* \cdot (\mathbf{V}^* c_m^*)]_{Convection} - [D_m^* \nabla^{*2} c_m^*]_{Diffusion} \tag{7}$$

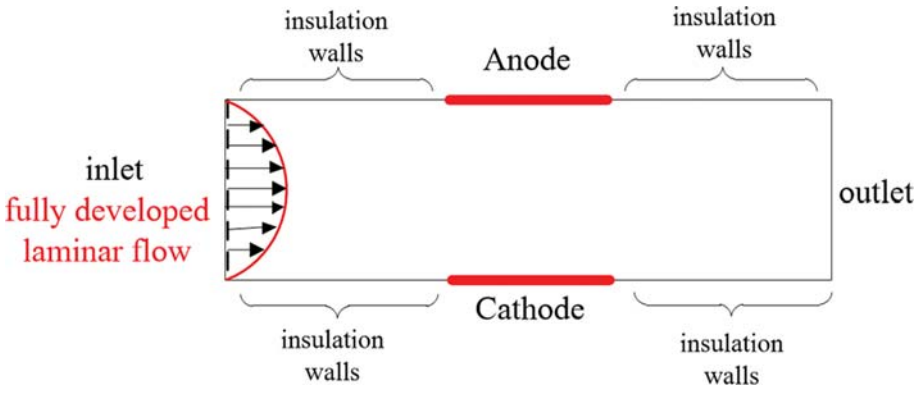

Fig. 1. Schematic of the different boundaries.

$$-[z_m D_m^* \{\nabla^* c_m^* \cdot \nabla^* \Phi^* + c_m^* \nabla^{*2} \Phi^*\}]_{Migration}$$

$$\sum_{m=1}^{p} z_m c_m^* = 0 \tag{8}$$

After solving Eqs. (7)-(8) and obtaining the distribution of the ionic concentration and electrolyte potential, the dimensionless form of total current density can be calculated by the following formula:

$$\mathbf{i}^* = \sum_{m=1}^{p} z_m \mathbf{N}_m^{* diff+mig} = \sum_{m=1}^{p} (-z_m D_m^* \nabla^* c_m^* - z_m^2 D_m^* c_m^* \nabla^* \Phi^*) \tag{9}$$

2. Electrochemical Boundary Conditions

All the boundaries used in this study are schematically shown in Fig. 1. As shown, there are four types of electrochemical boundary conditions: inlet, outlet, insulation walls, and electrodes (i.e., anode and cathode). In the following subsections, each electrochemistry-based boundary condition is explained in more detail.

2-1. Inlet Boundary Condition

At the fluid inlet, the concentration of all ionic species is equal to the amount of its bulk. In addition, normal gradient of potential at the boundary is zero. Thus:

$$c_m^*)_{inlet} = c_m^{*\infty} \tag{10}$$

$$\left(\frac{\partial \Phi^*}{\partial n^*}\right)_{inlet} = 0 \tag{11}$$

2-2. Outlet Boundary Condition

At the boundaries, normal gradients of concentration and potential are zero.

$$\left(\frac{\partial c_m^*}{\partial n^*}\right)_{outlet} = 0 \tag{12}$$

$$\left(\frac{\partial \Phi^*}{\partial n^*}\right)_{outlet} = 0 \tag{13}$$

2-3. Insulation Walls Boundary Condition

The electrochemical boundary conditions associated with insulation walls are as follows:

$$\frac{\partial c_m^*}{\partial n^*} = 0 \tag{14}$$

$$\frac{\partial \Phi^*}{\partial n^*} = 0 \tag{15}$$

2-4. At The Electrode Surfaces (Anode and Cathode)

In electrodes, the boundary conditions are different for reactive and neutral ionic species. The normal flux of the reactive ions is equal to the summation of the electrical current density generated during each electrochemical reaction.

- On the electrodes for reacting ion

$$-\mathbf{N}_m^{* diff+mig} \cdot n^* = \sum_{r=1}^{n_{reaction}} \xi \frac{S_{r,m} i_{n_r}^*}{n_r} \tag{16}$$

The additional parameter $\xi = -1$ in Eq. (16) has been introduced in order to consider a different sign convention that is typically used for current density in electrochemical literature. The dimensionless normal current density $i_{n_r}^*$ which generally depends on the solution variables is determined by (often nonlinear) kinetic models.

$$i_{n_r}^* = f(\eta_{s_r}, c_1, c_2, \ldots, c_m) \tag{17}$$

In Eq. (17), n_{s_r} is the surface over-potential which is the driving force of the electrochemical reactions.

$$\eta_{s_r} = (V_E - \Phi - E_r^{\infty}) \tag{18}$$

where V_E represents the electrode surface potential, Φ is the electric potential on the solution side of the electric double layer and E_r^{∞} represents the equilibrium open-circuit potential. An important example for Eq. (17) is the Butler-Volmer law:

$$i_{n_r}^* = i_{0_r}^* \left[\frac{c_m}{c_m^{\infty}}\right]^{\beta_{m,r}} \{\exp[\alpha_{a_r} n_r (V_E^* - \Phi^* - E_r^{*\infty})] - \exp[-\alpha_{c_r} n_r (V_E^* - \Phi^* - E_r^{*\infty})]\} \tag{19}$$

- On the electrodes for non-reacting ion

The normal flux is zero for ionic species that do not participate in reactions (neutral species):

$$\mathbf{N}_m^{* diff+mig} \cdot n^* = 0 \tag{20}$$

The boundary conditions in the electrodes are fulfilled along with the electro-neutrality condition. Note that, applied potential for electrochemical cell is equal to the potential difference between anode and cathode. In numerical simulations, the anode potential is usually considered zero for ease of calculation.

$$V_{applied} = V_A - V_C \tag{21}$$

3. Deposition Rate

The deposition rate and electrode growth velocity are defined by the current distribution on the electrode Surface. In electroplating applications, deposition rate at the cathode and the rate of dissolution at the anode are directly proportional to the current density [22].

The important point here is to specify what species are participating in the electrode reactions.

The total growth velocity is defined as the summation of velocity contributions for all species and electrode reactions:

$$V_{dep,\,total}[\mathrm{m/s}]=\sum_{m}\frac{M_m}{\rho_m}\sum_{r}\frac{S_{r,m}\mathbf{i}_{n_r}}{n_r F} \tag{22}$$

where $\mathbf{M}_m$ (SI unit: [kg/mol]) is the molar mass and ρ_m (SI unit: [kg/m^3]) is the density of the species m.

4. Fluid Flow

The distribution of the laminar parabolic velocity between two parallel plates is expressed as follows:

$$u=\frac{6u_{ave}}{h^2}y(h-y) \tag{23}$$

The characteristic velocity here is equal to $6u_{ave}$ and the characteristic length is equal to height of the channel. As a result, the dimensionless horizontal and vertical components of velocity are equal to:

$$u^*=-y^*(y^*-1) \tag{24}$$

$$v^*=0 \tag{25}$$

DISCRETIZATION METHODS

After writing the governing equations, diffusion and migration terms are discretized by the second-order accuracy central unequally spaced, but for the convection term, upwind method in combination with minimal artificial viscosity method [23] is utilized. To discretize the convection term, the half nodes must be introduced as shown in Fig. 2.

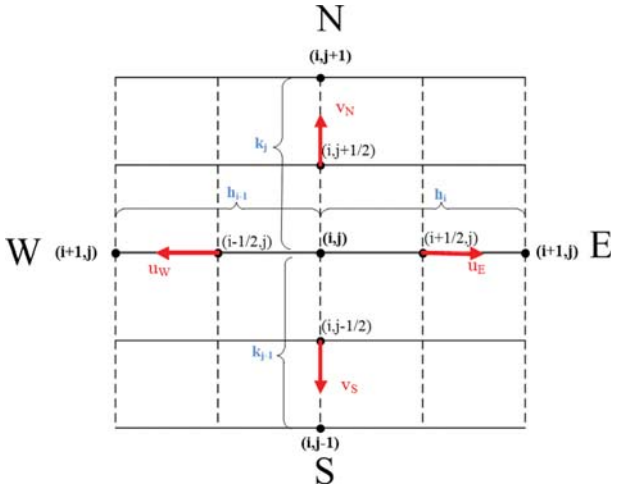

Fig. 2. Definition of velocities at half nodes using upwind differencing scheme for convection term.

Regarding the above mentioned, the convection term of the governing equation can be discretized as follows:

$$\begin{aligned}T_{conv}=&\left[\frac{Pe(h_i-h_{i-1})u^*_{i,j}}{h_ih_{i-1}}+\frac{Pe(k_j-k_{j-1})v^*_{i,j}}{k_jk_{j-1}}\right]c^*_{m_{i,j}}\\&+\left[\frac{Peh_{i-1}u_E}{h_i(h_i+h_{i-1})}\right]c^*_{m_{i+1,j}}-\left[\frac{Peh_iu_W}{h_{i-1}(h_i+h_{i-1})}\right]c^*_{m_{i-1,j}}\\&+\left[\frac{Pek_{j-1}v_N}{k_j(k_j+k_{j-1})}\right]c^*_{m_{i,j+1}}-\left[\frac{Pek_jv_S}{k_{j-1}(k_j+k_{j-1})}\right]c^*_{m_{i,j-1}}\end{aligned} \tag{26}$$

COUPLED MANNER SOLUTION OF PDEs

Due to the existence of nonlinear terms in the ionic transfer equation and the boundary condition in electrodes, nonlinear solvers must be used. In this study, we applied a coupled manner solver combined with Newton-Raphson method [21] which is schematically depicted in Fig. 3.

In the coupled manner, all the PDEs are discretized and solved simultaneously. The convergence criterion of the general system is checked at each iteration. Moreover, due to the existence of nonlinear terms, an outer iterate loop like Newton-Raphson is needed. To implement the coupled manner method, a node counter (k) based on the location of each node (i, j) must be defined as follows:

$$k=(j-1)N+i \tag{27}$$

In this equation, N represents the number of nodes in the horizontal direction.

1. Coupled Manner for Governing Equations

By rewriting the terms in the mass transfer Eqs. (7)-(8) using coupled manner method, the following relations will be achieved:

$$\begin{aligned}s(k,1)=&\left\{\left(\frac{2\mu_W^{(1)}h_i+2\mu_E^{(1)}h_{i-1}+Pe(h_i^2-h_{i-1}^2)u_k^*}{h_ih_{i-1}(h_i+h_{i-1})}\right)\right.\\&\left.+\left(\frac{2\mu_S^{(1)}k_j+2\mu_N^{(1)}k_{j-1}+Pe(k_j^2-k_{j-1}^2)v_k^*}{k_jk_{j-1}(k_j+k_{j-1})}\right)\right\}c^*_{1_k}\\&+\left(\frac{-2\mu_E^{(1)}h_{i-1}+Peh_{i-1}^2u_E}{h_ih_{i-1}(h_i+h_{i-1})}\right)c^*_{1_{k+1}}+\left(\frac{-2\mu_W^{(1)}h_i-Peh_i^2u_W}{h_ih_{i-1}(h_i+h_{i-1})}\right)c^*_{1_{k-1}}\\&+\left(\frac{-2\mu_N^{(1)}k_{j-1}+Pek_{j-1}^2v_N}{k_jk_{j-1}(k_j+k_{j-1})}\right)c^*_{1_{k+N}}+\left(\frac{-2\mu_S^{(1)}k_j-Pek_j^2v_S}{k_jk_{j-1}(k_j+k_{j-1})}\right)c^*_{1_{k-N}}\end{aligned}$$

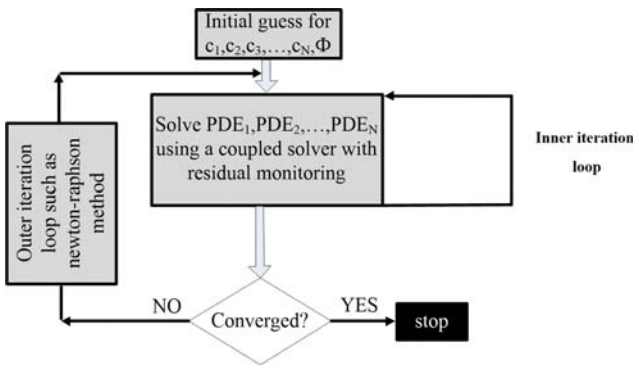

Fig. 3. Coupled manner algorithm used to solve coupled nonlinear PDEs [21].

$$-z_1 D_1^* \left\{ \begin{array}{l} \left[\left(\dfrac{h_{i-1}^2 c_{1_{k+1}}^* - h_i^2 c_{1_{k-1}}^* + (h_i^2 - h_{i-1}^2) c_{1_k}^*}{h_i h_{i-1}(h_i + h_{i-1})} \right) \right. \\ \left. \cdot \left(\dfrac{h_{i-1}^2 \Phi_{k+1}^* - h_i^2 \Phi_{k-1}^* + (h_i^2 - h_{i-1}^2) \Phi_k^*}{h_i h_{i-1}(h_i + h_{i-1})} \right) \right] \\ + \left[\left(\dfrac{k_{j-1}^2 c_{1_{k+N}}^* - k_j^2 c_{1_{k-N}}^* + (k_j^2 - k_{j-1}^2) c_{1_k}^*}{k_j k_{j-1}(k_j + k_{j-1})} \right) \right. \\ \left. \cdot \left(\dfrac{k_{j-1}^2 \Phi_{k+N}^* - k_j^2 \Phi_{k-N}^* + (k_j^2 - k_{j-1}^2) \Phi_k^*}{k_j k_{j-1}(k_j + k_{j-1})} \right) \right] \end{array} \right\} \quad (28)$$

$$-z_1 D_1^* c_{1_k}^* \left\{ \left(\frac{2h_{i-1}\Phi_{k+1}^* + 2h_i \Phi_{k-1}^* - 2(h_i + h_{i-1})\Phi_k^*}{h_i h_{i-1}(h_i + h_{i-1})} \right) + \left(\frac{2k_{j-1}\Phi_{k+N}^* + 2k_j \Phi_{k-N}^* - 2(k_j + k_{j-1})\Phi_k^*}{k_j k_{j-1}(k_j + k_{j-1})} \right) \right\}$$

$$s(k,2) = \left\{ \left(\frac{2\mu_W^{(2)} h_i + 2\mu_E^{(2)} h_{i-1} + Pe(h_i^2 - h_{i-1}^2) u_k^*}{h_i h_{i-1}(h_i + h_{i-1})} \right) + \left(\frac{2\mu_S^{(2)} k_j + 2\mu_N^{(2)} k_{j-1} + Pe(k_j^2 - k_{j-1}^2) v_k^*}{k_j k_{j-1}(k_j + k_{j-1})} \right) \right\} c_{2_k}^*$$
$$+ \left(\frac{-2\mu_E^{(2)} h_{i-1} + Peh_{i-1}^2 u_E}{h_i h_{i-1}(h_i + h_{i-1})} \right) c_{2_{k+1}}^* + \left(\frac{-2\mu_W^{(2)} h_i - Peh_i^2 u_W}{h_i h_{i-1}(h_i + h_{i-1})} \right) c_{2_{k-1}}^*$$
$$+ \left(\frac{-2\mu_N^{(2)} k_{j-1} + Pek_{j-1}^2 v_N}{k_j k_{j-1}(k_j + k_{j-1})} \right) c_{2_{k+N}}^* + \left(\frac{-2\mu_S^{(2)} k_j - Pek_j^2 v_S}{k_j k_{j-1}(k_j + k_{j-1})} \right) c_{2_{k-N}}^*$$

$$-z_2 D_2^* \left\{ \begin{array}{l} \left[\left(\dfrac{h_{i-1}^2 c_{2_{k+1}}^* - h_i^2 c_{2_{k-1}}^* + (h_i^2 - h_{i-1}^2) c_{2_k}^*}{h_i h_{i-1}(h_i + h_{i-1})} \right) \right. \\ \left. \cdot \left(\dfrac{h_{i-1}^2 \Phi_{k+1}^* - h_i^2 \Phi_{k-1}^* + (h_i^2 - h_{i-1}^2) \Phi_k^*}{h_i h_{i-1}(h_i + h_{i-1})} \right) \right] \\ + \left[\left(\dfrac{k_{j-1}^2 c_{2_{k+N}}^* - k_j^2 c_{2_{k-N}}^* + (k_j^2 - k_{j-1}^2) c_{2_k}^*}{k_j k_{j-1}(k_j + k_{j-1})} \right) \right. \\ \left. \cdot \left(\dfrac{k_{j-1}^2 \Phi_{k+N}^* - k_j^2 \Phi_{k-N}^* + (k_j^2 - k_{j-1}^2) \Phi_k^*}{k_j k_{j-1}(k_j + k_{j-1})} \right) \right] \end{array} \right\} \quad (29)$$

$$-z_2 D_2^* c_{2_k}^* \left\{ \left(\frac{2h_{i-1}\Phi_{k+1}^* + 2h_i \Phi_{k-1}^* - 2(h_i + h_{i-1})\Phi_k^*}{h_i h_{i-1}(h_i + h_{i-1})} \right) + \left(\frac{2k_{j-1}\Phi_{k+N}^* + 2k_j \Phi_{k-N}^* - 2(k_j + k_{j-1})\Phi_k^*}{k_j k_{j-1}(k_j + k_{j-1})} \right) \right\}$$

$$s(k,3) = z_1 c_{1_k}^* + z_2 c_{2_k}^* \quad (30)$$

where s(k, 1), s(k, 2) and s(k, 3) represent the residual of ionic charge conservation equation related to the ionic species 1 and 2 and electroneutrality, respectively. For each boundary condition the same procedure should be done.

NUMERICAL PROCEDURE

For solving nonlinear coupled PDEs using the coupled manner in combination with Newton-Raphson method, the following steps must be applied: First, the discretized form of governing equations and boundary conditions must be derived. Then, to apply the Newton-Raphson method, $dc_{1_k}^*$, $dc_{2_k}^*$ and $d\Phi_k^*$ should be defined which represent the variation of concentration of species 1 and 2 and potential at node k, respectively.

$$\begin{bmatrix} AP(k,1,1) & AP(k,1,2) & AP(k,1,3) \\ AP(k,2,1) & AP(k,2,2) & AP(k,2,3) \\ AP(k,3,1) & AP(k,3,2) & AP(k,3,3) \end{bmatrix} \begin{bmatrix} dc_{1_k}^* \\ dc_{2_k}^* \\ d\Phi_k^* \end{bmatrix}$$
$$+ \begin{bmatrix} AE(k,1,1) & AE(k,1,2) & AE(k,1,3) \\ AE(k,2,1) & AE(k,2,2) & AE(k,2,3) \\ AE(k,3,1) & AE(k,3,2) & AE(k,3,3) \end{bmatrix} \begin{bmatrix} dc_{1_{k+1}}^* \\ dc_{2_{k+1}}^* \\ d\Phi_{k+1}^* \end{bmatrix}$$
$$+ \begin{bmatrix} AW(k,1,1) & AW(k,1,2) & AW(k,1,3) \\ AW(k,2,1) & AW(k,2,2) & AW(k,2,3) \\ AW(k,3,1) & AW(k,3,2) & AW(k,3,3) \end{bmatrix} \begin{bmatrix} dc_{1_{k-1}}^* \\ dc_{2_{k-1}}^* \\ d\Phi_{k-1}^* \end{bmatrix} \quad (31)$$
$$+ \begin{bmatrix} AN(k,1,1) & AN(k,1,2) & AN(k,1,3) \\ AN(k,2,1) & AN(k,2,2) & AN(k,2,3) \\ AN(k,3,1) & AN(k,3,2) & AN(k,3,3) \end{bmatrix} \begin{bmatrix} dc_{1_{k+N}}^* \\ dc_{2_{k+N}}^* \\ d\Phi_{k+N}^* \end{bmatrix}$$
$$+ \begin{bmatrix} AS(k,1,1) & AS(k,1,2) & AS(k,1,3) \\ AS(k,2,1) & AS(k,2,2) & AS(k,2,3) \\ AS(k,3,1) & AS(k,3,2) & AS(k,3,3) \end{bmatrix} \begin{bmatrix} dc_{1_{k-N}}^* \\ dc_{2_{k-N}}^* \\ d\Phi_{k-N}^* \end{bmatrix} = \begin{bmatrix} -s(k,1) \\ -s(k,2) \\ -s(k,3) \end{bmatrix}$$

Eq. (31) is the general form of equations after applying the coupled manner in combination with Newton-Raphson method. The new coefficients in Eq. (31) are introduced in Table 1.

The numerical solution procedure used in the study is mentioned below:

1. Guess $\begin{bmatrix} c_{1_k}^* \\ c_{2_k}^* \\ \Phi_k^* \end{bmatrix}$ and $\begin{bmatrix} dc_{1_k}^* \\ dc_{2_k}^* \\ d\Phi_k^* \end{bmatrix}$ for all the nodes: the reasonable initial guess of $\begin{bmatrix} c_{1_k}^* \\ c_{2_k}^* \\ \Phi_k^* \end{bmatrix}$ can guaranty the convergence achievement.

2. Calculate $\begin{bmatrix} dc_{1_k}^* \\ dc_{2_k}^* \\ d\Phi_k^* \end{bmatrix}$ in inner iterate loop: Eq. (31) must be iterated till the convergence criterion (=10^{-6}) is obtained for each node.

3. Next guess $\begin{bmatrix} c_{1_k}^* \\ c_{2_k}^* \\ \Phi_k^* \end{bmatrix}$ after the inner iterate loop converges and the

Table 1. Definition of coefficients in Eq. (31)

$AP(k,1,1)=\frac{\partial s(k,1)}{\partial c^*_{1_k}}$	$AE(k,1,1)=\frac{\partial s(k,1)}{\partial c^*_{1_{k+1}}}$	$AW(k,1,1)=\frac{\partial s(k,1)}{\partial c^*_{1_{k-1}}}$	$AN(k,1,1)=\frac{\partial s(k,1)}{\partial c^*_{1_{k+N}}}$	$AS(k,1,1)=\frac{\partial s(k,1)}{\partial c^*_{1_{k-N}}}$
$AP(k,1,2)=\frac{\partial s(k,1)}{\partial c^*_{2_k}}$	$AE(k,1,2)=\frac{\partial s(k,1)}{\partial c^*_{2_{k+1}}}$	$AW(k,1,2)=\frac{\partial s(k,1)}{\partial c^*_{2_{k-1}}}$	$AN(k,1,2)=\frac{\partial s(k,1)}{\partial c^*_{2_{k+N}}}$	$AS(k,1,2)=\frac{\partial s(k,1)}{\partial c^*_{2_{k-N}}}$
$AP(k,1,3)=\frac{\partial s(k,1)}{\partial \Phi^*_k}$	$AE(k,1,3)=\frac{\partial s(k,1)}{\partial \Phi^*_{k+1}}$	$AW(k,1,3)=\frac{\partial s(k,1)}{\partial \Phi^*_{k-1}}$	$AN(k,1,3)=\frac{\partial s(k,1)}{\partial \Phi^*_{k+N}}$	$AS(k,1,3)=\frac{\partial s(k,1)}{\partial \Phi^*_{k-N}}$
$AP(k,2,1)=\frac{\partial s(k,2)}{\partial c^*_{1_k}}$	$AE(k,2,1)=\frac{\partial s(k,2)}{\partial c^*_{1_{k+1}}}$	$AW(k,2,1)=\frac{\partial s(k,2)}{\partial c^*_{1_{k-1}}}$	$AN(k,2,1)=\frac{\partial s(k,2)}{\partial c^*_{1_{k+N}}}$	$AS(k,2,1)=\frac{\partial s(k,2)}{\partial c^*_{1_{k-N}}}$
$AP(k,2,2)=\frac{\partial s(k,2)}{\partial c^*_{2_k}}$	$AE(k,2,2)=\frac{\partial s(k,2)}{\partial c^*_{2_{k+1}}}$	$AW(k,2,2)=\frac{\partial s(k,2)}{\partial c^*_{2_{k-1}}}$	$AN(k,2,2)=\frac{\partial s(k,2)}{\partial c^*_{2_{k+N}}}$	$AS(k,2,2)=\frac{\partial s(k,2)}{\partial c^*_{2_{k-N}}}$
$AP(k,2,3)=\frac{\partial s(k,2)}{\partial \Phi^*_k}$	$AE(k,2,3)=\frac{\partial s(k,2)}{\partial \Phi^*_{k+1}}$	$AW(k,2,3)=\frac{\partial s(k,2)}{\partial \Phi^*_{k-1}}$	$AN(k,2,3)=\frac{\partial s(k,2)}{\partial \Phi^*_{k+N}}$	$AS(k,2,3)=\frac{\partial s(k,2)}{\partial \Phi^*_{k-N}}$
$AP(k,3,1)=\frac{\partial s(k,3)}{\partial c^*_{1_k}}$	$AE(k,3,1)=\frac{\partial s(k,3)}{\partial c^*_{1_{k+1}}}$	$AW(k,3,1)=\frac{\partial s(k,3)}{\partial c^*_{1_{k-1}}}$	$AN(k,3,1)=\frac{\partial s(k,3)}{\partial c^*_{1_{k+N}}}$	$AS(k,3,1)=\frac{\partial s(k,3)}{\partial c^*_{1_{k-N}}}$
$AP(k,3,2)=\frac{\partial s(k,3)}{\partial c^*_{2_k}}$	$AE(k,3,2)=\frac{\partial s(k,3)}{\partial c^*_{2_{k+1}}}$	$AW(k,3,2)=\frac{\partial s(k,3)}{\partial c^*_{2_{k-1}}}$	$AN(k,3,2)=\frac{\partial s(k,3)}{\partial c^*_{2_{k+N}}}$	$AS(k,3,2)=\frac{\partial s(k,3)}{\partial c^*_{2_{k-N}}}$
$AP(k,3,3)=\frac{\partial s(k,3)}{\partial \Phi^*_k}$	$AE(k,3,3)=\frac{\partial s(k,3)}{\partial \Phi^*_{k+1}}$	$AW(k,3,3)=\frac{\partial s(k,3)}{\partial \Phi^*_{k-1}}$	$AN(k,3,3)=\frac{\partial s(k,3)}{\partial \Phi^*_{k+N}}$	$AS(k,3,3)=\frac{\partial s(k,3)}{\partial \Phi^*_{k-N}}$

$\begin{bmatrix} dc^*_{1_k} \\ dc^*_{2_k} \\ d\Phi^*_k \end{bmatrix}$ distribution is achieved in all nodes, then the next guess for $\begin{bmatrix} c^*_{1_k} \\ c^*_{2_k} \\ \Phi^*_k \end{bmatrix}$ can be obtained from the following relations:

$$\begin{aligned} c^{*\,n+1}_{1_k} &= c^{*\,n}_{1_k} + (W \cdot dc^{*\,n}_{1_k}) \\ c^{*\,n+1}_{2_k} &= c^{*\,n}_{2_k} + (W \cdot dc^{*\,n}_{2_k}) \\ \Phi^{*\,n+1}_k &= \Phi^{*\,n}_k + (W \cdot d\Phi^{*\,n}_k) \end{aligned} \tag{32}$$

where superscripts (n+1) and (n) represent the guess at the new and previous step, respectively, and (W) expresses the relaxation factor which can be smaller or larger than one. This loop is referred to as the outer iterate loop.

4. Outer iterate loop convergence: the iteration process should be continued till the outer iterate loop convergence criteria are achieved and the value of $\begin{bmatrix} dc^*_{1_k} \\ dc^*_{2_k} \\ d\Phi^*_k \end{bmatrix}$ at each node becomes zero.

RESULTS AND DISCUSSION

In this research, seven cases were used to investigate the effect of location and size of electrodes on electrochemical parameter. Fig. 4 shows the schematic of a parallel plate electrochemical reactor as case 1.

The grid used for all numerical simulation is an unequally spaced

Table 2. Diffusion coefficient of species [16]

Ion number	Ion name	Diffusion coefficient [m^2/s]
1	Cu^{2+}	7.20E-10
2	SO_4^{2-}	10.65E-10

Table 3. Input parameters [16]

Reaction	$E_r^{*\infty}$	i_{0_r} [A/m^2]	α_{a_r}	α_{c_r}	$\beta_{m,r}$	$S_{r,m}$	T [°k]	Sc
1,2	0[a]	30	0.5	0.5	1	−1	298	1633

[a]Versus a reference electrode of the same kind as the anode.

Table 4. Peclet numbers used in this study

Item	Re	$Pe=3ScRe\frac{(w+h)}{h}$	u_{ave} [m/s]
1	0.000186	1	12×10^{-9}
2	0.001856	10	12×10^{-8}
3	0.01855	100	12×10^{-7}
4	0.18	1000	12×10^{-6}
5	1.85	10^4	12×10^{-5}
6	18.55	10^5	12×10^{-4}
7	154.63	8.33×10^5	0.01
8	700	3.77×10^6	0.04526
9	1300	7×10^6	0.084
10	2100	11.3×10^6	0.1358

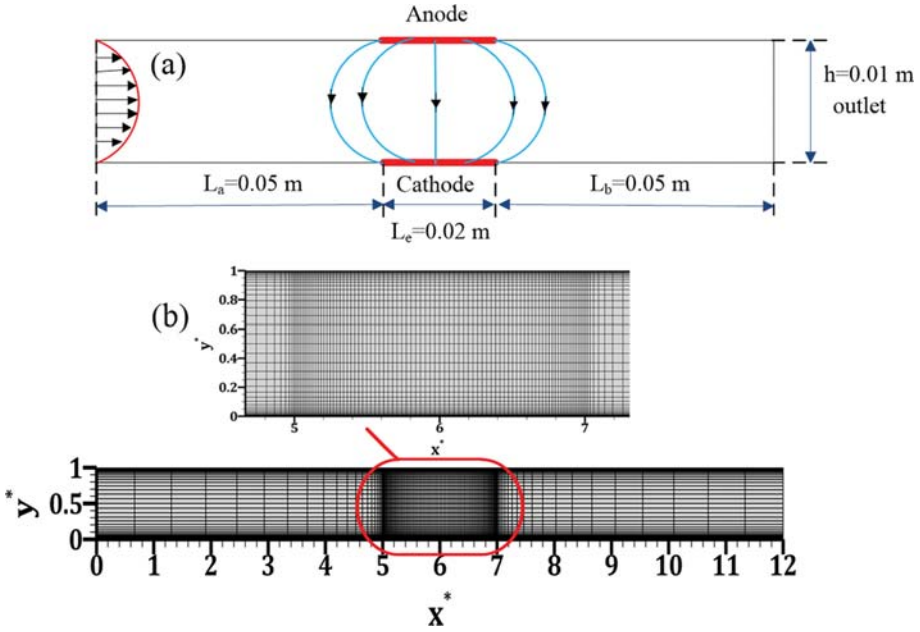

Fig. 4. (a) Geometry of case 1 (b) mesh generation and zoom of the grid in the electrode realm of case 1.

rectangular mesh with 4961 nodes (121 nodes in the x-direction and 41 nodes in the y-direction). To challenge the huge concentration gradients, nodes are concentrated in the vicinity of electrodes and their leading and trailing edges. Nine nodes were placed in a layer of 5.0e-4 [m] electrode surfaces to make sure that the concentration boundary layer was properly modeled. A zoom of the grid in the electrodes realm of case 1 is given in Fig. 4(b). The constant coefficients used in this research are presented in Table 2 and Table 3.

For each case in the beginning of modeling, the small applied potential cell is implemented and in each applied potential cell, the average of current density is calculated on the cathode and anode. The calculations continue till there is no change in average of current density between two consecutive potential steps, called the limiting current density.

Distribution of concentration, potential, current density and concentration boundary layer thickness under fluid flow is calculated for various Peclet numbers as presented in Table 4.

In Fig. 5 distribution of normalized concentration Cu^{2+} on the cathode and anode is depicted in various fractions of the limiting current density. The results show there is a good agreement between present work and results of multidimensional upwind method [16]. Moreover, by increasing applied cell voltage, the concentration of Cu^{2+} on the cathode is reduced and it increases on the anode.

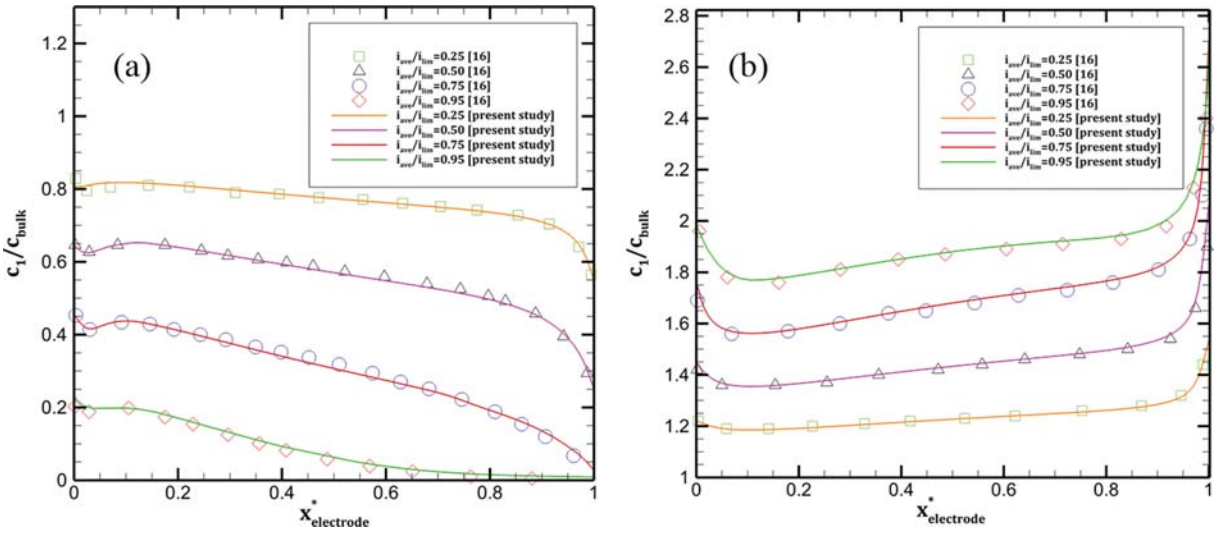

Fig. 5. Normalized concentration distribution at various limiting current density fractions for case 1 on the (a) cathode, (b) anode (u_{ave}=0.01 [m/s]).

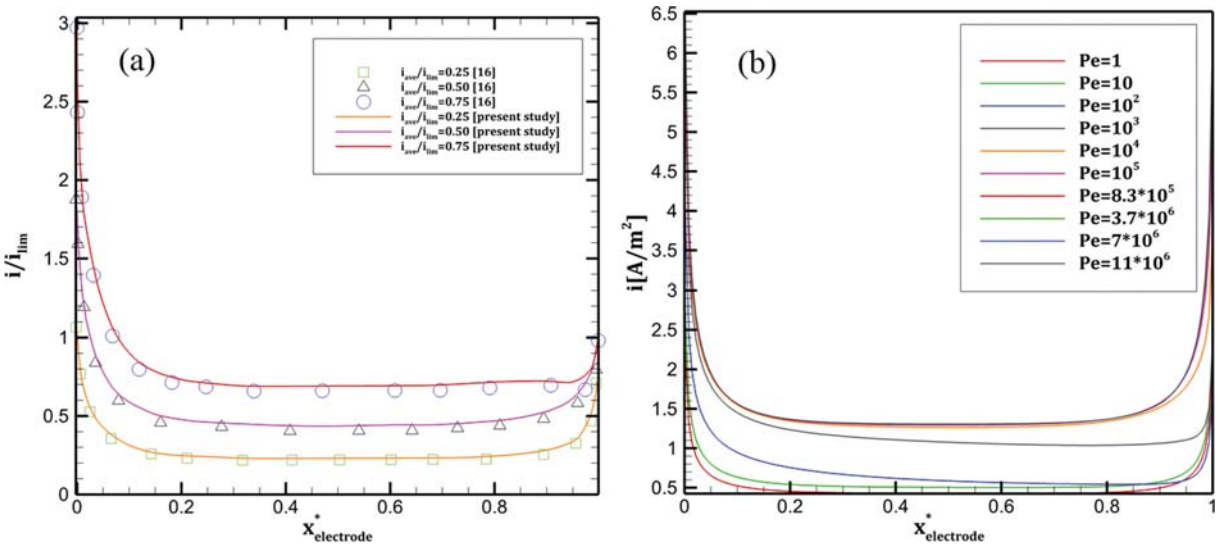

Fig. 6. (a) Normalized current distribution on the cathode at various fractions of the limiting current density (b) current density on the cathode at various Peclet numbers in V_{app}=−50 mv.

From Fig. 5(a), it is obvious that the concentration of copper on the cathode getting close to zero is a sign of approaching the limiting current density.

Fig. 6(a) presents the variation of normalized current density on the cathode for different limiting current density fractions. Evidently, the modeling results agreed very well with the results of multidimensional upwind method [16]. Furthermore, by increasing the length of cathode, a sudden drop in current density distribution will occur, which is due to the high concentration gradient due to Cu^{2+} ion depletion. As illustrated in Fig. 6(a), by an increment of the applied potential cell, current density and consequently the deposition rate increases. This procedure will continue until the limiting current density is achieved. After this situation, with adding more applied potential, no more change in the current density occurs and it will be fixed. Fig. 6(b) presents the variation of current density on the cathode at various Peclet numbers. As shown in Fig. 6(b), at a specified applied potential cell, by increasing inlet velocity, the current density on the cathode increases. Between Pe=1 and Pe=10^4, this increment is very evident. But with more increase in Peclet number between Pe=10^4 and Pe=$11*10^6$, the current density is almost fixed. So, to enhance the current density and deposition rate under the limiting current density condition, the electrolyte velocity can be increased to a certain range, thereafter it will not actually be effective.

Fig. 7 illustrates the dimensionless concentration of Cu^{2+} contours for different Peclet numbers. With an increment of Peclet number, the concentration contours are pushed to downstream and they become thinner. At low Peclet numbers, the concentration gradient in electrode realm is governed by diffusion, whereas in Peclet numbers between 10^2 and 10^4, the effect of convection dominates and the concentration gradient is limited to a smaller vertical distance from the electrode surface. As a result, the concentration boundary layer thickness decreases dramatically with the increase in Peclet number.

In Fig. 8 the concentration boundary layer thickness of Cu^{2+} on

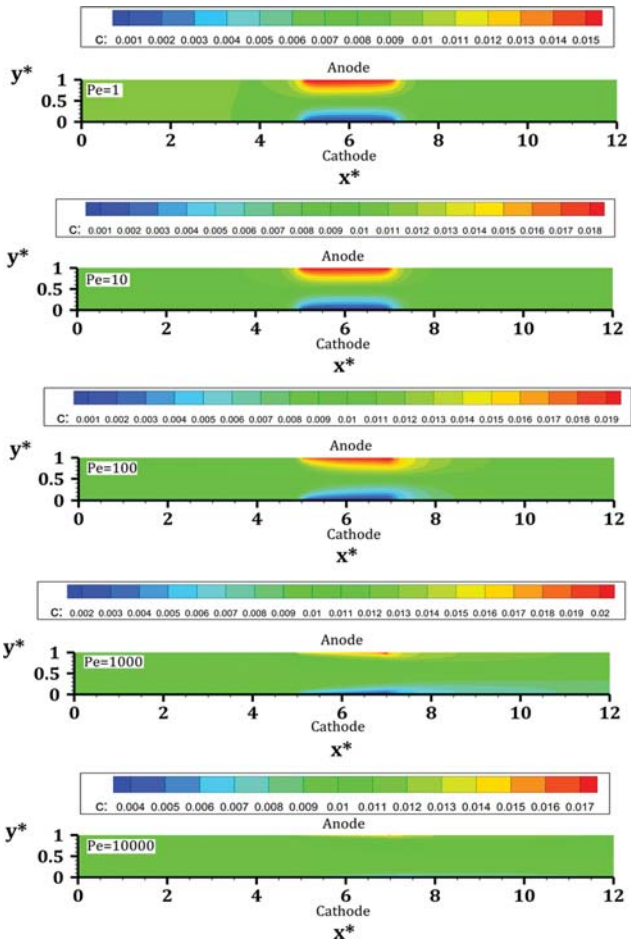

Fig. 7. Dimensionless concentration contours for case 1 at various Peclet numbers in V_{app}=−50 mv.

the cathode in different Peclet numbers has been plotted. As shown, at low Peclet numbers, such as 10 and 10^2, the thickness of the con-

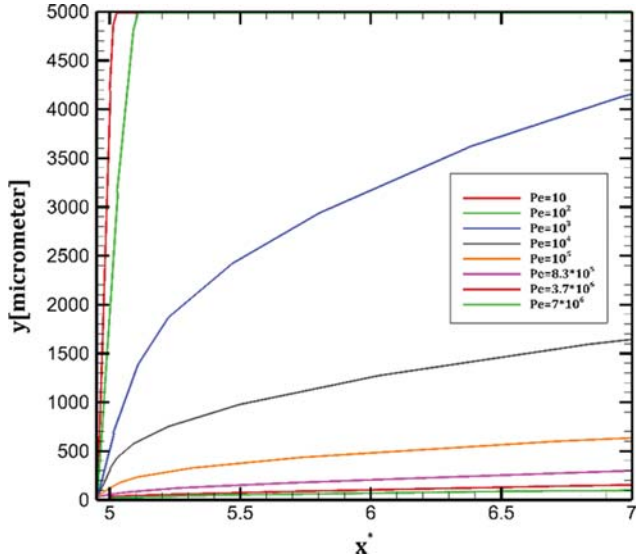

Fig. 8. Concentration boundary layer thickness on the cathode at various Peclet numbers in V_{app}=−50 mv.

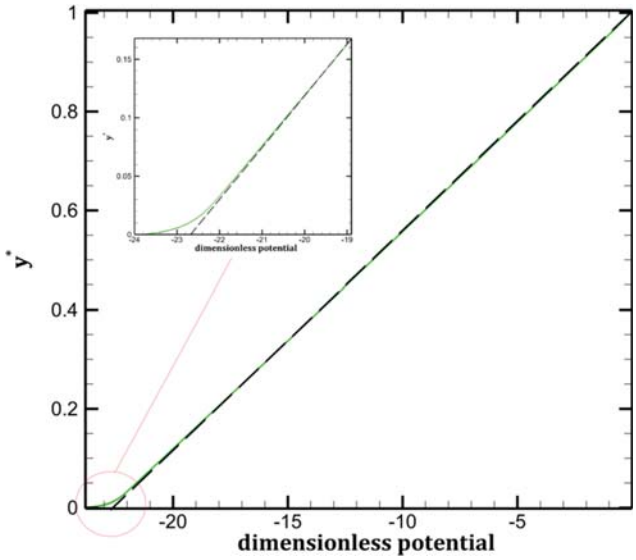

Fig. 10. Dimensionless potential distribution within the height of channel of middle point of electrodes in case 1 (u_{ave}=0.01 m/s, V_{app}=650 mv). (dashed line: by solving Laplace equation) (green line: by solving governing equation).

centration boundary layer has its maximum value which reaches up to the half of the channel height. In this situation, the concentration boundary layers formed on the cathode and anode touch each other. Thus, the concentration profile varies across the channel height and actually there is no bulk. Under such conditions, Laplace's equation for the electric potential in electrolyte cannot be used. Although with increase in mass transfer effect (due to convection), this thickness decreases. For example, at Pe=8.3×10^5, the concentration boundary layer thickness is about 300 micrometers.

In Fig. 9(a) the normalized concentration distribution of Cu^{2+} within the height of channel in the middle point of the electrodes for various Peclet numbers is plotted. At very low velocities, which correspond to the low Peclet numbers, concentration varies across the channel and there is no bulk region in the electrolyte. By increasing Peclet number, concentration variations are confined to the electrode realm (concentration boundary layer), and in other areas the concentration is equal to the bulk value. Another notable point is that by reducing the Peclet number, the concentration of Cu^{2+} on the cathode tends to zero at lower applied potential cell. Thus, at lower applied potentials, the limiting current density occurs. Fig. 9(b) shows the normalized concentration of Cu^{2+} within height of the channel at three points: the first, middle and end point of the electrodes. As can be seen, except very limited vertical distances of the electrodes, Cu^{2+} concentration is equal to the bulk value. Moreover, in the simulation, no concentration over-potential is introduced. As the simulation continues, the concentration boundary layer appears as a natural result of modeling. The concentration of species outside of the concentration boundary layer remains con-

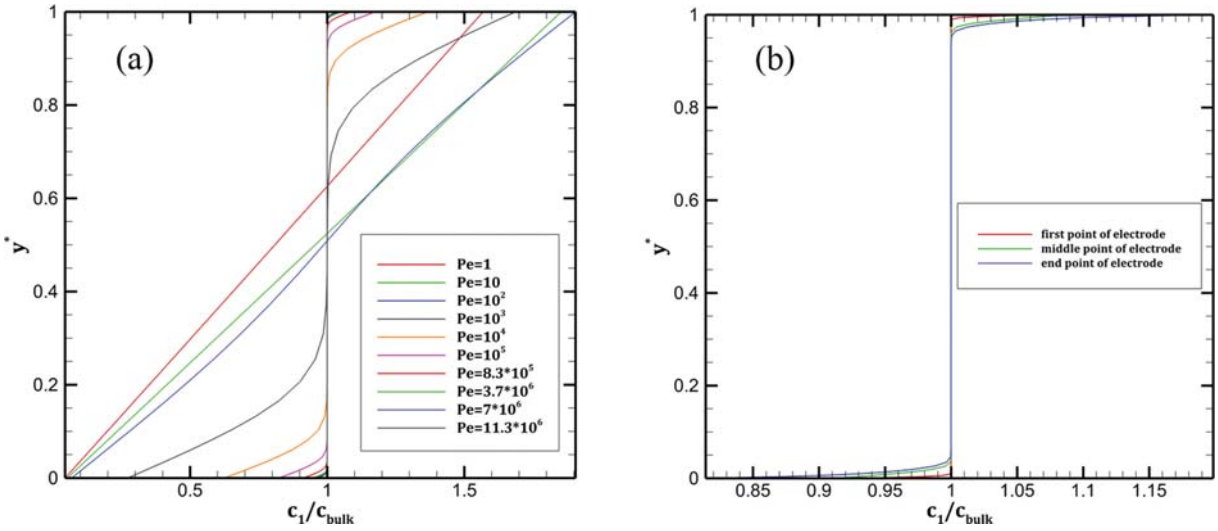

Fig. 9. Normalized concentration distribution of Cu^{2+} within the height of channel at V_{app}=50 mv. (a) In the middle point of electrodes in various Peclet numbers (b) at u_{ave}=0.01 m/s in 3 points of electrodes.

stant. Consequently, in this region the governing equations reduce to Laplace's equations for electric potential.

The presented computational method can consider the three effects of ohmic over-potential, concentration over-potential and surface over-potential. The surface over-potential is a result of the Butler-Volmer equation for kinetics of electrode, while ohmic and concentration over-potentials are automatically added by the coupled ion-transport equations. In Fig. 10, the potential distribution through the height of the channel is depicted. In the bulk electrolyte solution, the ohmic over-potential causes a linear potential profile behavior which is shown by the dashed line. Inside the concentration boundary layer, concentration over-potential causes a nonlinear potential profile (green line). It must be emphasized that the influence of the concentration over-potential is much smaller

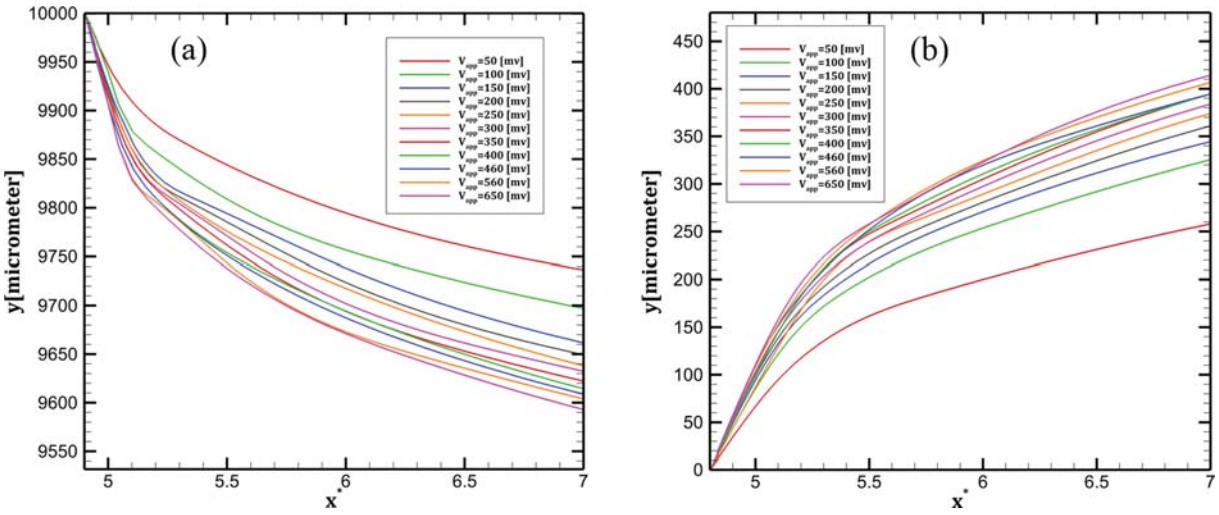

Fig. 11. Concentration boundary layer thickness at various applied potential cell in case 1 at u_{ave}=0.01 m/s on the (a) anode, (b) cathode.

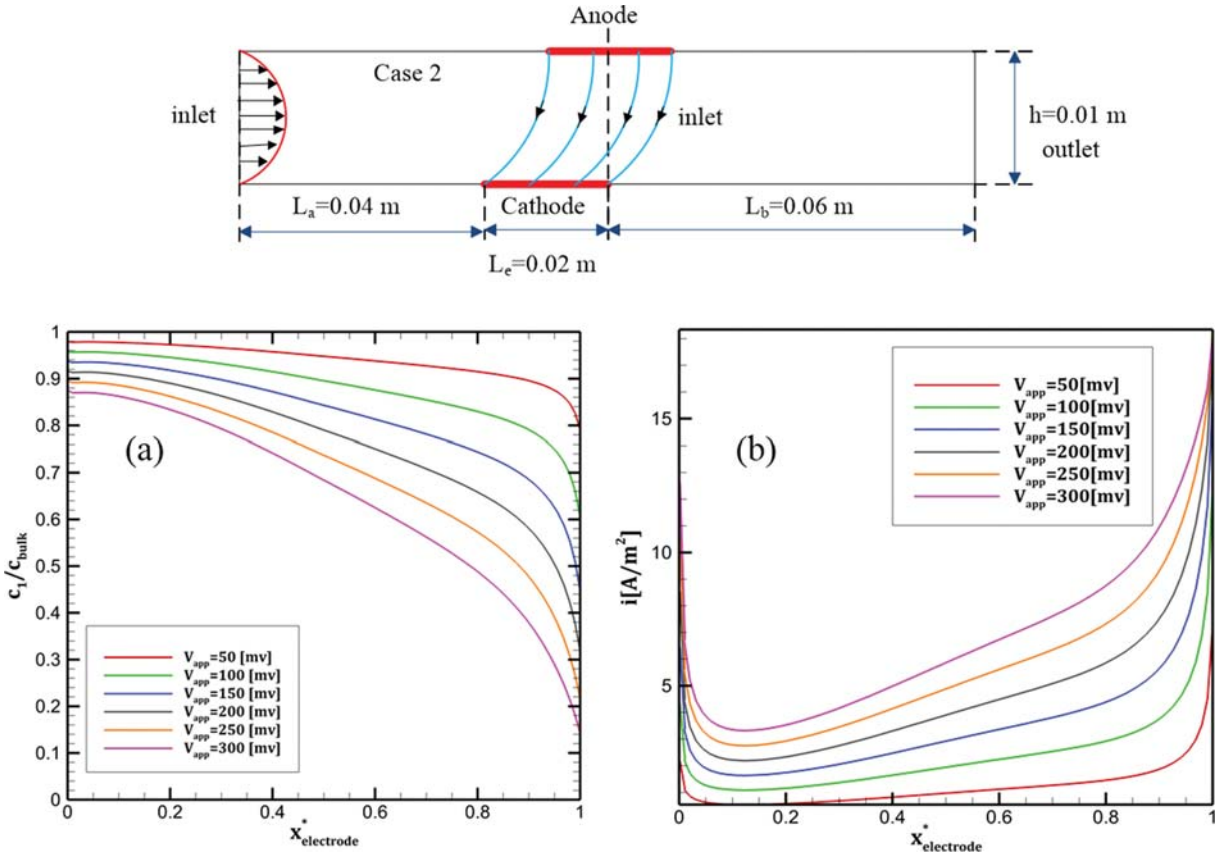

Fig. 12. View of case 2 at various applied potential cell and u_{ave}=0.01 m/s (a) Normalize concentration (b) current density on the cathode.

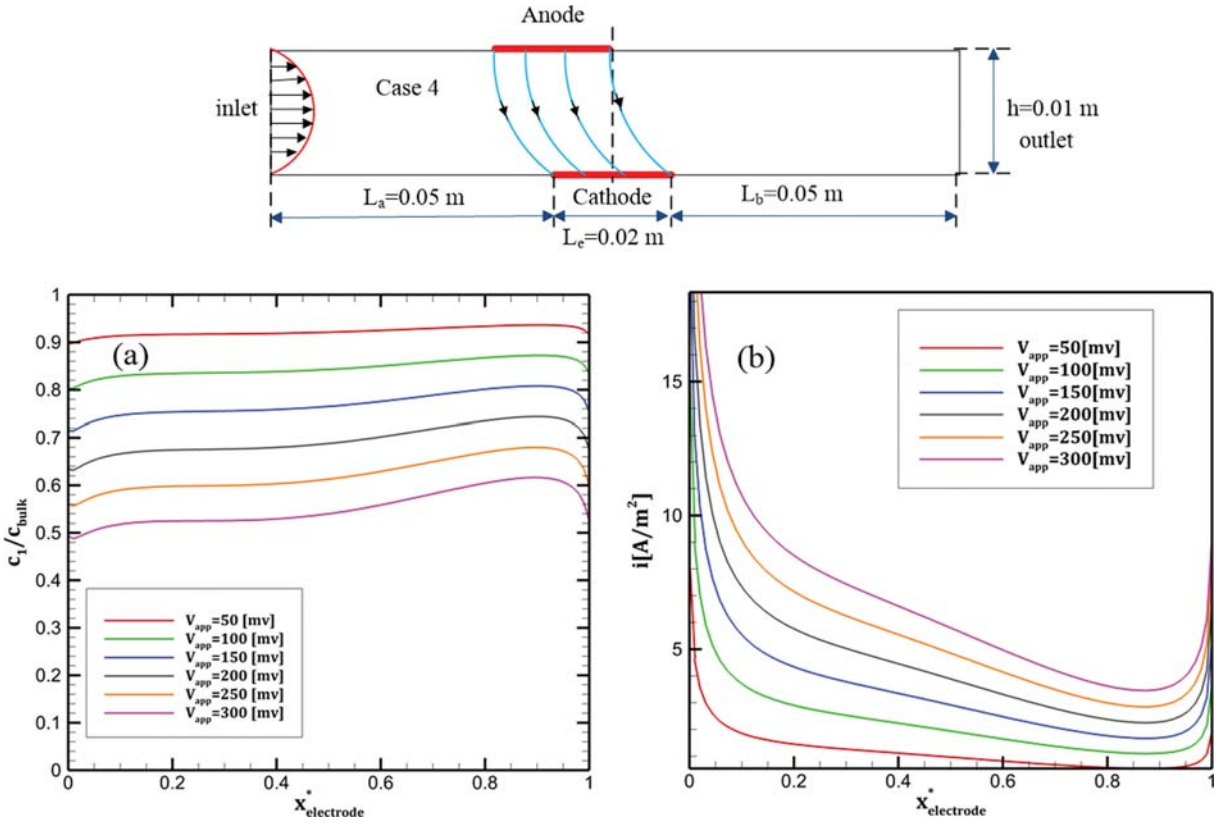

Fig. 13. View of case 4 at various applied potential cell u_{ave}=0.01 m/s and (a) Normalize concentration (b) current density on the cathode.

at the anode.

Fig. 11 shows concentration boundary layer thickness at anode and cathode for various applied potential cells. An increment of applied potential cell increases the thickness of the concentration boundary layer in the anode and cathode. As can be seen in Fig. 11(a) and 11(b), by approaching the limiting current density, the growth rate of the boundary layer thickness decreases.

In this study, cases 2-5 were used to investigate the influence of electrode position on concentration and current density distribution. In case 2, as can be seen in Fig. 12, the cathode was placed $L_{electrode}/2$ before than anode, but in the case 3, as can be seen in Fig. S1 in the supporting Information, this value was doubled. The opposite pattern was implemented in cases 4 and 5 as can be seen in Fig. 13 and Fig. S2 in the supporting Information.

According to results of cases 2 and 3 (Fig. 12(a) and Fig. S1(a)) and compared with result of case 1, in a specific applied potential cell, the concentration of Cu^{2+} on the cathode has more values. So, the average of current density and deposition rate on the cathode is reduced. As can be seen from Fig. 12(b), the current density on the right side of the cathode is higher than the left side and consequently more deposited thicknesses can be expected in this area. By comparing the results between cases 2 and 3, as the cathode moves in the opposite direction of the electrolyte flow, the maximum of current density is shifted to the right side of the cathode. Therefore, the left regions of the cathode are less affected by electrochemical processes.

By comparison of results between cases 2 and 4, it can be concluded that due to the mass transfer caused by convection, the concentration of reactive ion on the cathode in case 4 is smaller than case 2. Thus, the average of current density and deposition rate in case 4 and 5 due to convection effect is more than case 2 and 3.

Fig. 13 shows an overview of case 4. In this case, the cathode was placed $L_{electrode}/2$ ahead of the anode, but in Fig. S2 in the supporting Information, this value was doubled. As shown in Fig. 13(b) and Fig. S2(b), the current density on the left side of the cathode is higher than the right side and consequently more deposited thicknesses can be expected in this area. By comparing the results between Fig. 13(a) and Fig. S2(a), as the cathode moves further from the anode, the concentration of Cu^{2+} on the right regions of the cathode is less affected by electrochemical processes and its value is closer to the bulk.

The effect of electrode size on the concentration and current density distribution is presented in Fig. S3 and Fig. S4 in the supporting Information. As illustrated in Fig. S3, it is considered that the anode size is twice as much as the cathode size, whereas in Fig. S4, it is vice versa. By comparing the results of case 6 and case 1, as anode size doubled, the average of total current density on the cathode rose significantly. Referring to Fig. S3(b), the maximum values of current density occur at the leading and trailing edges of cathode. It is expected that the thickness of the deposited layer increases in this area. By comparing the results of case 7 and case 1, it is determined that as cathode size doubled, the average of total current density on the cathode decreased significantly. Referring to Fig. S4(b), the maximum values of current density occur at

the center of cathode. It is forecast that the thickness of the deposited layer increases at the center of cathode. By comparing Fig. S3(a) and Fig. S4(a), it is evident that as anode size increases, the concentration of Cu^{2+} on the cathode decreases sharply and at lower applied potential cell its value approaches to zero (limiting current density).

CONCLUSIONS

A robust numerical scheme was applied for analysis of electrochemical systems governed by fully coupled nonlinear partial differential equations. The effects of fluid flow along with the phenomenological electrode-kinetic were considered. Electric potential, concentration and current density distributions and concentration boundary layer thickness were obtained for various Peclet numbers and applied potential cell. It was shown that the proposed numerical simulation can satisfactorily predict the behavior of the corresponding electrochemical system at low and high Peclet numbers. The proposed method has been successfully tested for seven cases to investigate the comprehensive behavior of the electrochemical systems. Increases of current density and deposition rate on the cathode caused by applied potential cell increment have been well observed. Moreover, it is concluded that the increase of current density due to increasing fluid flow velocity is clearly visible for Peclet numbers between 1 and 10^4. But, for Peclet numbers between 10^4 and $11*10^6$, the current density almost remains unchanged. Thus, to enhance the current density, fluid velocity can only be increased to a certain range. Also, complete studies were conducted on the effects of fluid velocity on the boundary layer thickness. Another key parameter in design of electrochemical systems is locating the position where current density is extremum. The size and configuration of the anode and cathode can change the location of maximum and minimum amount of the current density. In the present work the size and configuration of anode and cathode were changed for several cases and it was concluded that the proposed modeling can easily determine where and how the extremum occurs.

ACKNOWLEDGEMENTS

This work was supported by Shahid Chamran University of Ahvaz (Grant no. SCU.EM98.709). The authors would also like to appreciate the Gas Networks Research Center of Shahid Chamran University of Ahvaz for sharing its facilities during the course of this research.

NOMENCLATURE

$\mathbf{c}_m$: concentration of species m [mol/m^3]
$\mathbf{c}_{ref}$: characteristic concentration, c_{ref}=1000 [mol/m^3]
$\mathbf{c}_m^*$: dimensionless concentration of species m $c_m^* = \frac{c_m}{c_{ref}}$
$\mathbf{c}_m^\infty$: bulk concentration of species m [mol/m^3]
$\mathbf{c}_m^{*\infty}$: dimensionless bulk concentration of species m, $c_m^{*\infty} = \frac{c_m^\infty}{c_{ref}}$
$\mathbf{c}_{1_k}^*$: dimensionless concentration of species 1 at node k
$\mathbf{c}_{2_k}^*$: dimensionless concentration of species 2 at node k
$\mathbf{D}_m$: diffusion coefficient of species m [m^2/s]
$\mathbf{D}_{ref}$: characteristic diffusion coefficient, D_{ref}=7.2E-10 [m^2/s]
$\mathbf{D}_m^*$: dimensionless diffusion coefficient of species m, $D_m^* = \frac{D_m}{D_{ref}}$
$\mathbf{E}_r^\infty$: equilibrium open circuit potential of reaction r [volt]
$\mathbf{E}_r^{*\infty}$: dimensionless equilibrium open circuit potential of reaction r, $E_r^{*\infty} = \frac{E_r^\infty}{\Phi_{ref}}$
F : faraday's constant, F=96485.34 [C/mol]
h : height of channel [m]
$\mathbf{h}_i$: step of computational mesh in x-direction at node (i, j)
$\mathbf{i}$: total electric current density [A/m^2]
$\mathbf{i}^*$: dimensionless of total current density, $i^* = \frac{iL_{ref}}{FD_{ref}c_{ref}}$
$\mathbf{i}_{0_r}$: exchange current density of reaction r [A/m^2]
$\mathbf{i}_{n_r}$: normal current density of reaction r [A/m^2]
$\mathbf{i}_{n_r}^*$: dimensionless normal current density of reaction r, $i_{n_r}^* = \frac{i_{n_r}L_{ref}}{FD_{ref}c_{ref}}$
$\mathbf{k}_j$: step of computational mesh in y-direction at node (i, j)
$\mathbf{L}_{ref}$: characteristic length, L_{ref}=h
$\mathbf{v}^*$: dimensionless vertical component of velocity, $v^* = \frac{v}{U_{ref}}$
$\mathbf{V}_E^*$: dimensionless electrode surface potential, $V_E^* = \frac{V_E}{\Phi_{ref}}$
w : width of channel, w=0.1 [m]
$\mathbf{x}$: horizontal direction [m]
$\mathbf{x}^*$: dimensionless of horizontal direction, $x^* = \frac{x}{L_{ref}}$
$\mathbf{x}_{electrode}^*$: dimensionless of electrode length
$\mathbf{y}$: vertical direction [m]
$\mathbf{y}^*$: dimensionless of vertical direction, $y^* = \frac{y}{L_{ref}}$
$\mathbf{z}_m$: charge number of species m
μ_m : absolute mobility of species m
Φ : electrolyte potential [volt]
Φ^* : dimensionless of electrolyte potential, $\Phi^* = \frac{\Phi}{\Phi_{ref}}$
Φ_k^* : dimensionless of electrolyte potential at node k
$\mathbf{N}_m$: flux vector of species m [mol/m^2·s]
$\mathbf{N}_m^*$: dimensionless flux vector of species m
n^* : dimensionless direction normal to the boundary
n_r : number of electrons transferred in reaction r
Pe : Peclet number, $Pe = \frac{U_{ref}L_{ref}}{D_{ref}}$
R : universal gas constant, R=8.314462 [J/k·mol]
Re : Reynolds number, $Re = \frac{4u_{ave}wL_{ref}}{2\nu(w+L_{ref})}$
Sc : Schmidt number, $Sc = \frac{\nu}{D_{ref}}$
$S_{r,m}$: stoichiometric coefficient of species m in reaction r
T : electrolyte temperature [k]

T_{conv} : convection term in governing equation
u_{ave} : average of inlet velocity [m/s]
U_{ref} : characteristic velocity, Uref =6u_{ave}
u^* : dimensionless horizontal component of velocity, $\left(u^* = \frac{u}{U_{ref}}\right)$
u_E : east horizontal velocity, $u_E = u^*_{i+\frac{1}{2},j} = \frac{u^*_{i,j} + u^*_{i+1,j}}{2}$
u_W : west horizontal velocity, $u_W = u^*_{i-\frac{1}{2},j} = \frac{u^*_{i,j} + u^*_{i-1,j}}{2}$
$\mathbf{V}$: vector of velocity [m/s]
$\mathbf{V}^*$: dimensionless velocity, $\mathbf{V}^* = \frac{V}{U_{ref}}$
v_N : north vertical velocity, $v_N = v^*_{i,j+\frac{1}{2}} = \frac{v^*_{i,j} + v^*_{i,j+1}}{2}$
v_S : south vertical velocity, $v_S = v^*_{i,j-\frac{1}{2}} = \frac{v^*_{i,j} + v^*_{i,j-1}}{2}$
V_A : anode potential [volt]
V_C : cathode potential [volt]
Φ_{ref} : characteristic potential, $\Phi_{ref} = \frac{RT}{F}$ [Volt]
∇ : del operator
∇^* : dimensionless of del operator, $\nabla^* = L_{ref} \cdot \nabla$
ν : kinematic viscosity [m^2/s]
η_{s_r} : surface overpotential of reaction r [volt]
ρ_0 : electrolyte density [kg/m^3]
α_{a_r} : anodic transfer coefficient of reaction r
α_{c_r} : cathodic transfer coefficient of reaction r
$\beta_{m,r}$: constant order of species m in reaction r
$\mu_E^{(m)}$: east artificial viscosity of species m,

$$\mu_E^{(m)} = \max\left\{D_m^*,\ \mathrm{Peh}_{i-1}\frac{|u_E|}{2}\right\}$$

$\mu_W^{(m)}$: west artificial viscosity of species m,

$$\mu_W^{(m)} = \max\left\{D_m^*,\ \mathrm{Peh}_{i}\frac{|u_W|}{2}\right\}$$

$\mu_N^{(m)}$: north artificial viscosity of species m,

$$\mu_N^{(m)} = \max\left\{D_m^*,\ \mathrm{Pek}_{j-1}\frac{|v_N|}{2}\right\}$$

$\mu_S^{(m)}$: south artificial viscosity of species m,

$$\mu_S^{(m)} = \max\left\{D_m^*,\ \mathrm{Pek}_{j}\frac{|v_S|}{2}\right\}$$

SUPPORTING INFORMATION

Additional information as noted in the text. This information is available via the Internet at http://www.springer.com/chemistry/journal/11814.

REFERENCES

1. J. Dukovic, *IBM J. Res. Dev.*, **34**, 693 (1990).
2. K. I. Popov, P. M. Zivkovic and N. Nikolić, *J. Serb. Chem. Soc.*, **76**, 805 (2011).
3. U. Landau, *Modern Aspects of Electrochemistry*, **44**, 451 (2009).
4. M. Georgiadou, *Electrochim. Acta*, **48**, 4089 (2003).
5. H. Kawamoto, *J. Appl. Electrochem.*, **22**, 1113 (1992).
6. J. Newman, K. E. Thomas-Alyea, *Electrochemical systems*, John Wiley & Sons, Hoboken (2012).
7. K. Kontturi, L. Murtomäki and J. A. Manzanares, *Ionic transport processes: In electrochemistry and membrane science*, Oxford University Press, Oxford (2008).
8. J. H. Kim, Y. S. Kim and J. G. Kim, *Ocean Eng.*, **115**, 149 (2016).
9. A. Ehrl, G. Bauer, V. Gravemeier and W. A. Wall, *J. Comput. Phys.*, **235**, 764 (2013).
10. R. Struijs, H. Deconinck and P. Roe, in *Computational fluid dynamics*, H. Deconinck Ed., von Karman Institute for Fluid Dynamics, Belgium (1991).
11. S. Lorenzi, T. Pastore, T. Bellezze and R. Fratesi, *Corros. Sci.*, **108**, 36 (2016).
12. J. Lee and J. Selman, *J. Electrochem. Soc.*, **129**, 1670 (1982).
13. R. E. White, M. Bain and M. Raible, *J. Electrochem. Soc.*, **130**, 1037 (1983).
14. M. Buoni and L. Petzold, *J. Comput. Phys.*, **229**, 379 (2010).
15. I. E. Henley and A. C. Fisher, *J. Phys. Chem.*, **B 107**, 6579 (2003).
16. L. Bortels, J. Deconinck and B. Van Den Bossche, *J. Electroanal. Chem.*, **404**, 15 (1996).
17. M. Georgiadou, *J. Electrochem. Soc.*, **144**, 2732 (1997).
18. G. Nelissen, A. Van Theemsche, C. Dan, B. Van den Bossche and J. Deconinck, *J. Electroanal. Chem.*, **563**, 213 (2004).
19. V. Volgin and A. Davydov, *Russ. J. Electrochem.*, **37**, 1197 (2001).
20. G. Bauer, V. Gravemeier and W. A. Wall, *Int. J. Numer. Meth. Eng.*, **86**, 1339 (2011).
21. S. Mazumder, *Numerical methods for partial differential equations: Finite difference and finite volume methods*, Academic Press, London (2015).
22. G. Bauer, *A coupled finite element approach for electrochemical systems*, Ph.D thesis, Technische Universität München (2012).
23. P. J. Roache, *Computational fluid dynamics*, Hermosa Publishers, New Mexico (1972).

Supporting Information

Fluid flow effects on diffusion layer and current density for electrochemical systems

Behzad Ebadi[*,], Morteza Behbahani-Nejad[*,**,†], Maziar Changizian[*,**], and Ioan Pop[***]**

*Department of Mechanical Engineering, Faculty of Engineering,
Shahid Chamran University of Ahvaz, 61357-83151, Ahvaz, Iran
**Gas Networks Research Center, Shahid Chamran University of Ahvaz, 61357-83151, Ahvaz, Iran
***Department of Mathematics, Faculty of Mathematics and Computer Science,
Babeş-Bolyai University, 400084 Cluj-Napoca, Romania
(*Received 14 November 2019 • Revised 12 March 2020 • Accepted 12 April 2020*)

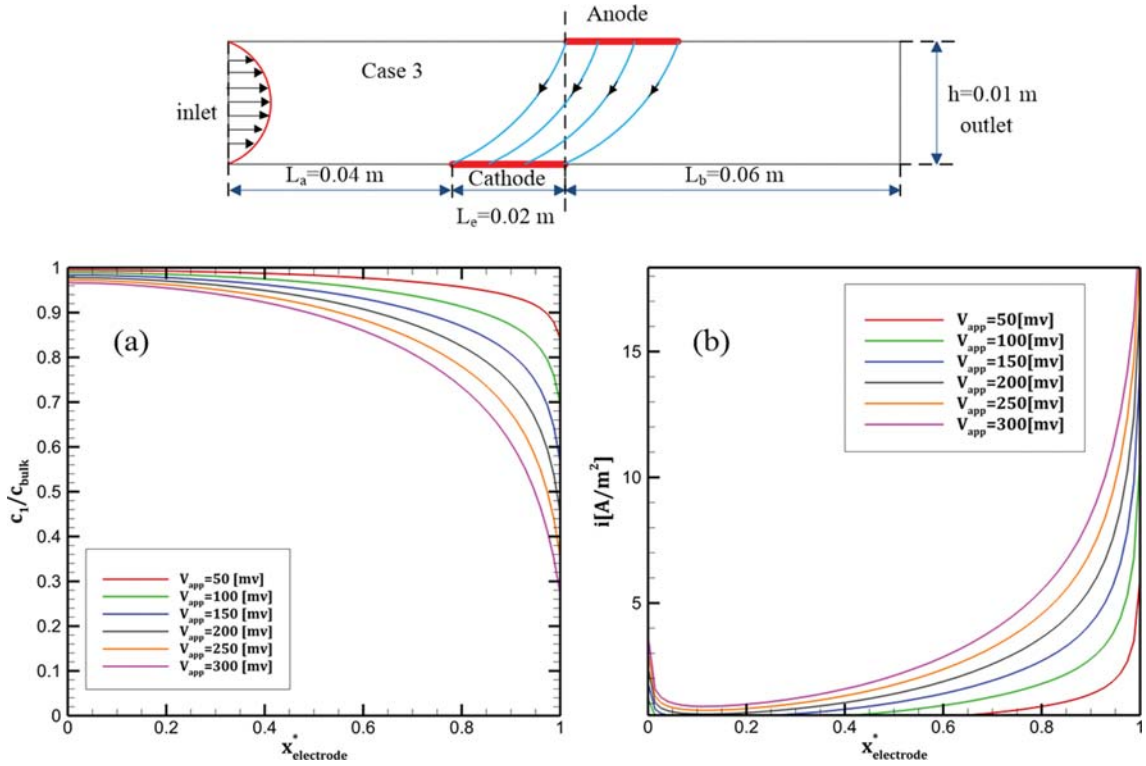

Fig. S1. View of case 3 at various applied potential cell and u_{ave}=0.01 m/s (a) Normalize concentration on the cathode, (b) current density on the cathode.

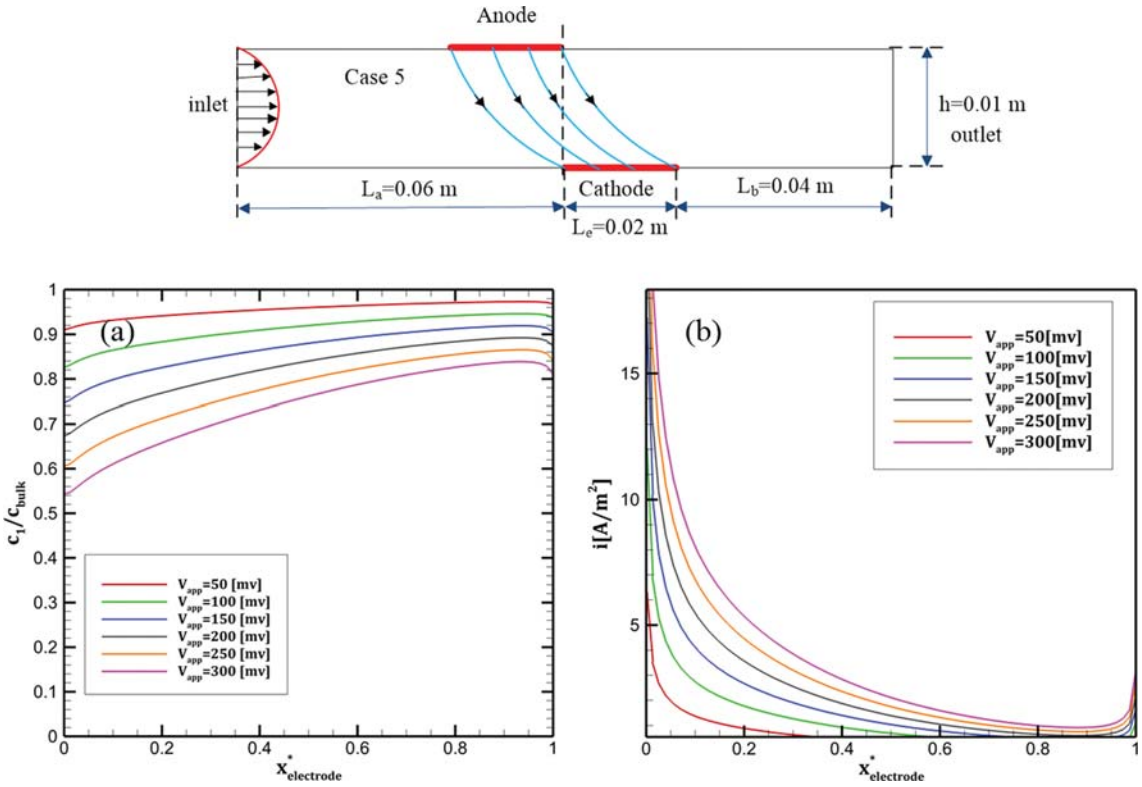

Fig. S2. View of case 5 at various applied potential cell and u_{ave}=0.01 m/s (a) Normalize concentration on the cathode, (b) current density on the cathode.

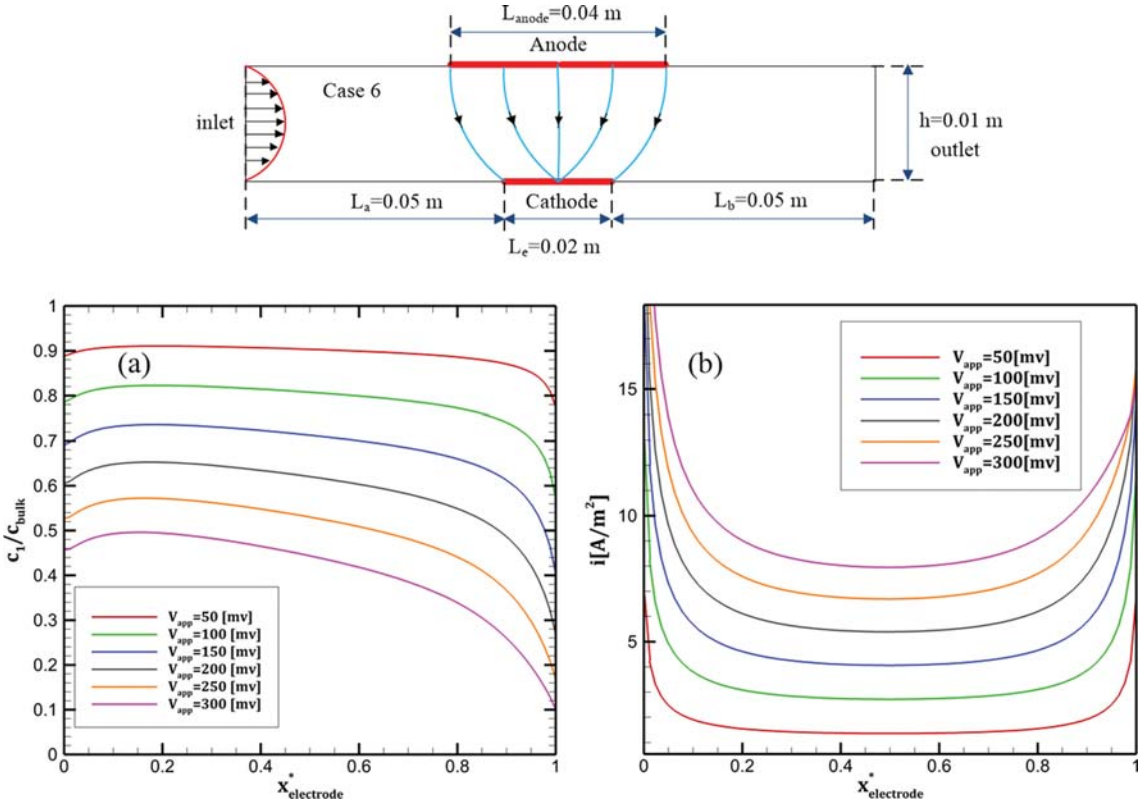

Fig. S3. View of case 6 at various applied potential cell and u_{ave}=0.01 m/s (a) Normalize concentration on the cathode, (b) current density on the cathode.

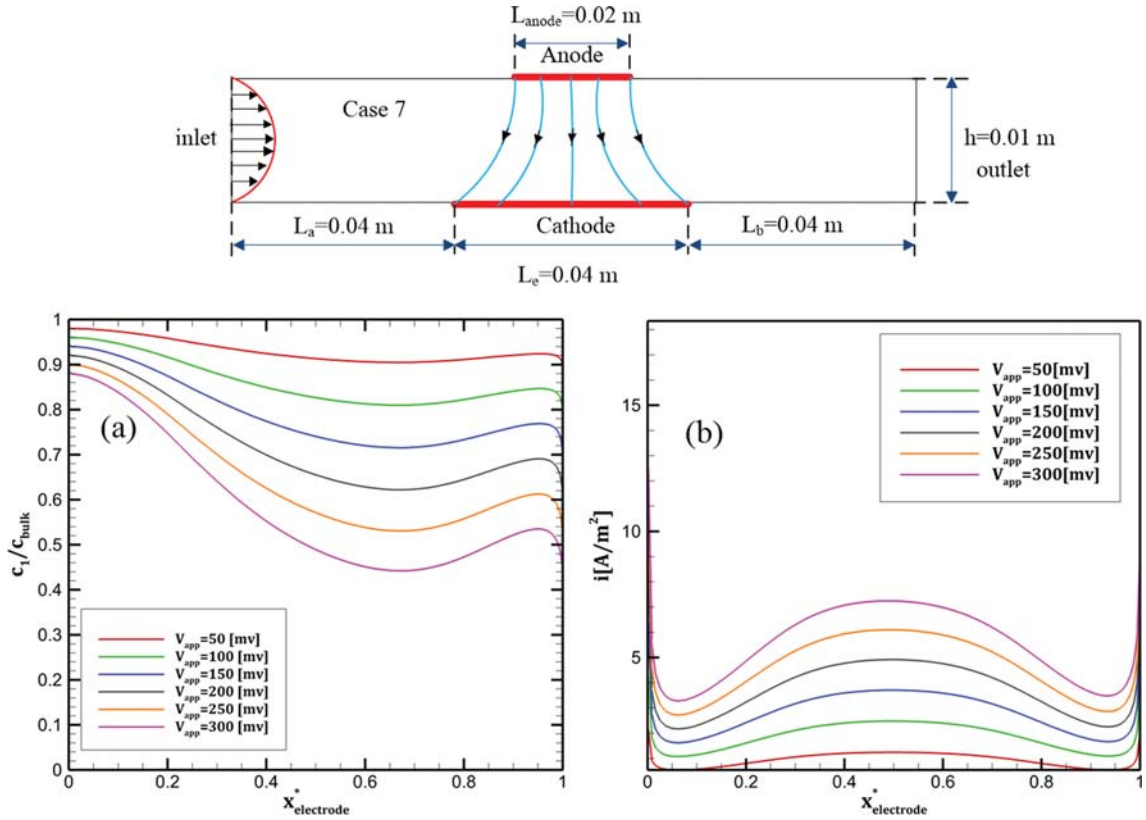

Fig. S4. View of case 7 at various applied potential cell and u_{ave}=0.01 m/s (a) Normalize concentration on the cathode, (b) current density on the cathode.